communications earth & environment

Article

https://doi.org/10.1038/s43247-024-01793-x

A drop in Antarctic sea ice extent at the end of the 1970s

Check for updates

Hugues Goosse [1] ✉, Quentin Dalaiden [1], F. Feba [1], Bianca Mezzina [1] & Ryan L. Fogt [2]

After a period of relative stability, the Antarctic sea ice extent has abruptly decreased in 2016 and has remained low since then. Both atmospheric and oceanic processes likely contributed to this drop but many questions remain regarding the underlying dynamics and it is unknown if this drop is unprecedented. Here we produce a new multi-variate spatial reconstruction covering 1958–2023 and show that a similar drop in sea ice extent occurred at the end of the 1970s, albeit with a smaller magnitude. Both drops show similar spatial patterns, with a higher sea ice loss in the East Antarctic sector than in the West Antarctic sector where the variability is strongly modulated by wind-driven changes. The ocean integrates the atmospheric forcing and provides memory that amplifies the magnitude of both drops.

Since 1979, corresponding to the onset of continuous estimates derived from satellite observations, the Antarctic sea ice extent has first slightly increased, reaching its highest annual mean value in 2014 before a dramatic decrease in 2016, leading to a record low in 2023[1–3]. These recent changes are so large that it has been suggested that sea ice has now shifted to a new regime compared to the period covering the late 20th century and the beginning of the 21st century[3,4].

Several studies have demonstrated the role of changes in atmospheric circulation in driving the recent sea ice loss but different origins have been identified for the different minima[5–8]. Furthermore, the transition from a positive to negative trend in sea ice extent in 2016 does not correspond to any observed shifts in the dominant modes of atmospheric variability influencing the Antarctic sea ice, such as the Southern Annular Mode (SAM), the Zonal wave mode 3 (ZW3) or El Niño Southern Oscillation[1,3,4,9]. This has led to the suggestion that the Southern Ocean warming observed since the 2015 may have been an important contributor to the maintenance of a low Antarctic sea ice extent[3,10–12].

The period covered by satellite observations is relatively short to describe the dynamics of a system like the Southern Ocean characterized by strong variability at all timescales[13]. Several sea ice reconstructions are available prior the satellite era, based on long instrumental observations and indirect climate records[14–19]. However, a quantitative comparison with recent changes is difficult because of the larger uncertainties in those reconstructions and spurious trends in some of them due to the increasing number of data with time[16,20]. Furthermore, those sea ice reconstructions have been produced independently of estimates of past oceanic and atmospheric variations, which complicates the description of the mechanisms responsible for the past sea ice changes.

Here, we show that a large sea ice extent decrease occurred just before the beginning of continuous satellite observations and we quantitatively compare the changes in sea ice, ocean and atmosphere during that period with the ones observed after 2016. To do so, we reconstruct spatial fields southward of 45°S for the period 1958–2023 by combining continuous atmospheric pressure and temperature observations from 27 ground-based weather stations (Supplementary Table 1) with results from nine large ensembles of coupled climate model simulations[21] (Supplementary Table 2) using data assimilation.

Results

Reconstructing changes over the period 1958–2023

The reconstruction method is based on a particle filter[19,22,23] in which each simulated state from the climate model ensembles receives a weight proportional to its similarity to observations. The reconstruction is then provided by the weighted mean of the different model states, the link between observation sites and locations where no observation is available and between observed and non-observed variables being based on model physics. The atmospheric reconstruction is then used to force the sea ice-ocean model NEMO to estimate the oceanic variations. This approach provides physically consistent estimates for all the fields for the atmosphere, sea ice and ocean. The reconstruction is also totally homogenous over the period covered as the same number of data series is used throughout and our method does not require a calibration period, thus avoiding potential biases and issues related to the non-stationarity out of this calibration period.

While the sea ice interannual variability is strongly seasonally dependent[1,18,24], the long-term trends are much more homogenous across seasons with, for example, the drop in sea ice extent after 2016 being

[1]Earth and Life Institute, Université catholique de Louvain, Louvain-la-Neuve, Belgium. [2]Department of Geography and Scalia Laboratory for Atmospheric Analysis, Ohio University, Athens, OH, USA. ✉e-mail: hugues.goosse@uclouvain.be

observed in all individual months or seasons[2,3,18]. This indicates that our reconstruction, which has an annual resolution, is well adapted to study these long-term trends[25]. Reconstructions have been generated using nine different coupled climate models, which overestimate or underestimate the observed sea ice extent, but our main conclusions are robust and remain valid independently of those biases (Supplementary Tables 3–4). As we find no objective reason to select one reconstruction over the others, we choose to use the multi-model reconstruction, which is derived from the average of the reconstructions obtained using the individual model results, in the following analyses.

The reconstruction of the assimilated variables is by design very close to the local temperature and sea level pressure station data used to constrain it (Fig. 1). To evaluate our reconstruction in regions distant from those stations, we have compared our results with ERA5 atmospheric reanalysis data[26] over the period 1979–2023, which provides a spatially complete field based on a large array of observations. For the multi-model reconstruction of sea level pressure (Fig. 1a), the correlation with ERA5 is higher than 0.75 nearly everywhere at high latitudes. As a consequence, a large-scale index such as the SAM index is also accurately reconstructed, with a correlation of 0.90 over the period 1958–2023 (Supplementary Fig. 1). The correlations are also larger than 0.5 in most regions for temperature (Fig. 1b), with values larger than 0.75 for regions with many stations. Consistently, the agreement of our reconstructions with pressure and temperature at the weather stations is as good for the period 1958–1979 as for the period 1979–2023, since the same data and procedure is used for the whole period of the reconstruction. By contrast, the correlation between our reconstruction and ERA5 is higher for the years 1979–2023 than for the years 1958–1979. ERA5 uses much less observations before 1979 than after 1979 and this lower agreement with our reconstruction over 1958–1979 may underline some limitations of ERA5 over Antarctica for this period[27,28] (Supplementary Fig. 2).

The skill for the variables that are not assimilated is generally lower in data assimilation-based estimates but remains high here for sea ice concentration nearly everywhere compared to NSIDC observations[29] (Fig. 1c). This evaluation provides an independent validation of our results, as no sea ice data are used at any stage in the reconstruction process. The sea ice extent has also been assessed for the different sectors of the Southern Ocean, obtaining correlations of the multi-model reconstruction with observations between 0.55 and 0.71 for all sectors (Supplementary Table 3, Supplementary Fig. 3). Reproducing the integrated sea ice extent over the whole Southern Ocean is more challenging because of complex spatial patterns as well as partial compensations between regions[1,18]. Nevertheless, the correlation between the multi-model reconstruction of the total Antarctic sea ice extent and observations over the period 1979–2023 reaches 0.56 (Fig. 2a). Despite this overall reasonable performance, our reconstructions tend to underestimate the magnitude of the extreme events, in particular the maximum extent in 2014 and the minimum in 2023. However, when utilizing our atmospheric reconstructions based on the CESM1-LM and CanESM2 ensembles to force NEMO, the correlation of the simulated Antarctic sea ice extent with NSIDC increases to values of 0.68 and 0.60, respectively (Fig. 2b, c). The long-term trends are also stronger, leading to slightly larger values in 2014 and lower values in 2023 in the NEMO simulations than for the CESM-LM1-based and CanESM2-based reconstructions.

The drops in sea ice extent at the end of the 1970s and in 2016

Our reconstruction is characterized by a negative trend in sea ice extent from 1958 to the end of the 1970s, followed by the slightly positive trend until 2015 described in many studies based on satellite records[2,29–31]. This leads to a difference in sea ice extent between the 1958–1979 and 1980–2015 periods that reaches 0.43 million km^2 in the multi-model reconstruction (Supplementary Table 4). The amplitude of this statistically significant drop is consistent across all the reconstructions (the range of the reconstructions based on different simulation ensembles is 0.22–0.58 million km^2) but smaller than the drop between 1980–2015 and 2016–2023, which is 0.69 million km^2 for the multi-model mean (the range of the reconstructions is

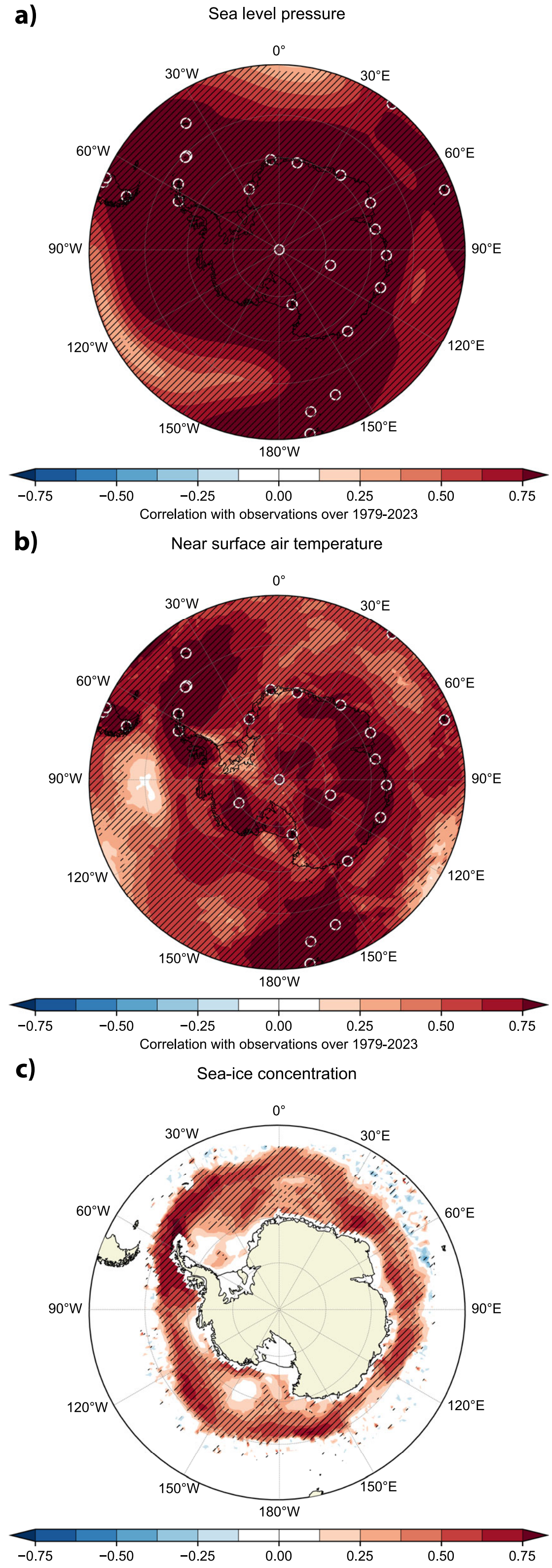

Fig. 1 | Skill of the reconstruction. The Pearson correlation of the multi-model reconstruction is shown for (**a**) annual mean sea level pressure and (**b**) near surface air temperature, with ERA5 reanalysis[26] and (**c**) the reconstruction of sea ice concentration with NSIDC[29] data over the period 1979–2023. Regions with a significant correlation at a 95% confidence level based on two-sided t-test, accounting for the autocorrelation of the series, are hatched. The correlation with weather station data is indicated in color inside the white circles (all significant at the 95% confidence level).

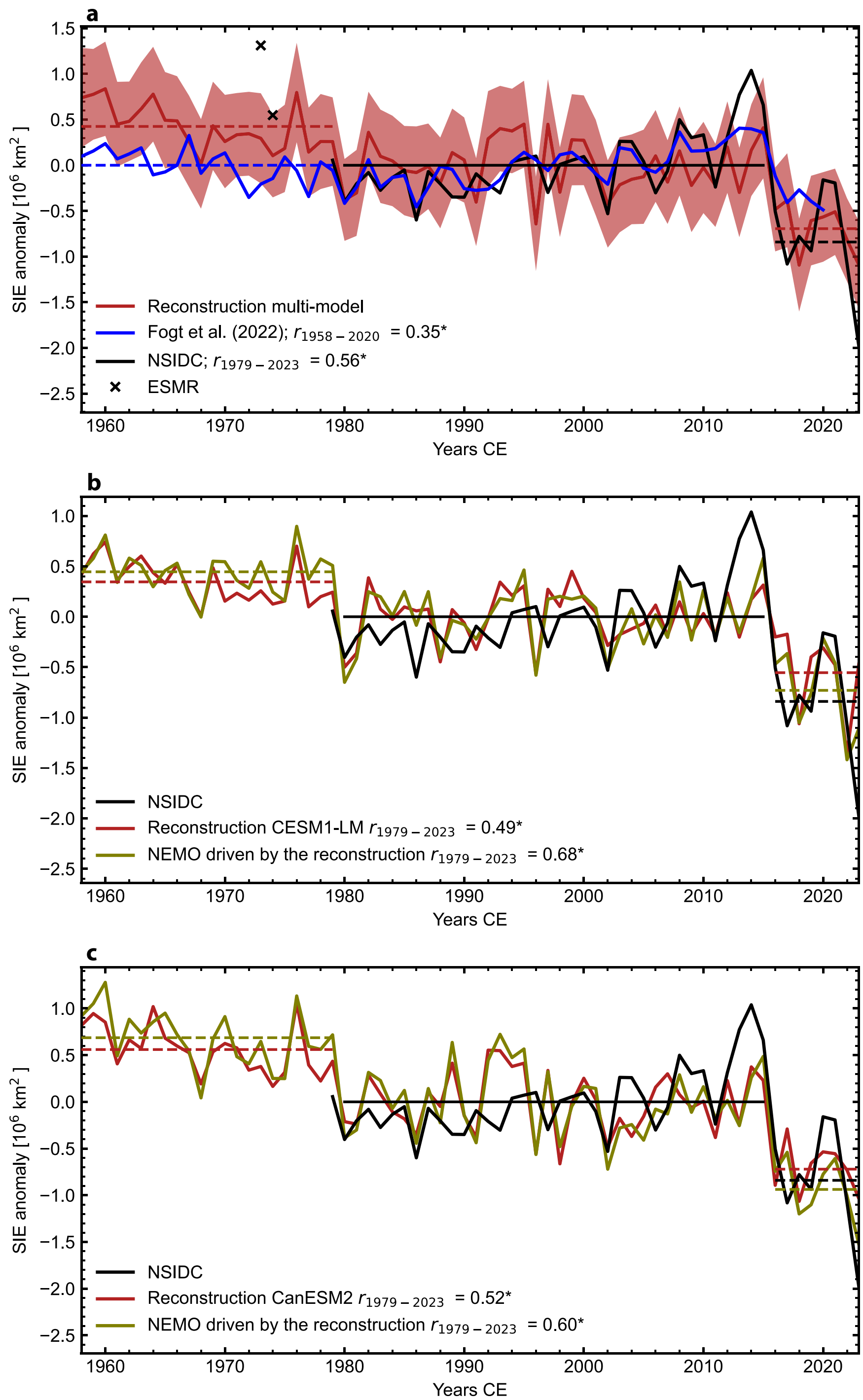

Fig. 2 | Time series of sea ice extent.
a Reconstruction of the annual mean Antarctic sea ice extent anomalies in the multi-model reconstruction (in red) compared with NSIDC[29] data (in black), the reconstruction of Fogt et al.[18] (in blue) and ESMR data[32] for the years 1973 and 1974 (black crosses). The red shading corresponds to one standard deviation of the ensemble reconstruction. **b** Reconstruction of the annual mean Antarctic sea ice extent anomalies based on CESM1-LM simulation ensemble and **c** CanESM2 simulation ensemble and simulations with NEMO driven by a forcing derived from those reconstructions (in olive green). A dashed line represents the mean over the periods 1958–1979 and 2016–2023 for the estimates that include these full periods. Anomalies are computed compared to the period 1980–2015 (solid lines). Correlations between the reconstruction and NSIDC data are given for the period 1979–2023 and correlation with Fogt et al.[18] for the period 1958–2020. All the correlations are significant at the 95% level based on two-sided *t*-test, accounting for the autocorrelation of the series.

0.30–1.0 million km^2), compared to an observed drop of 0.84 million km^2. The differences are higher in the NEMO simulations compared to the reconstruction used to generate the forcing by about 0.1 million km^2, bringing the model results closer to observations for the recent drop. Those drops are a robust characteristic of the multi-model reconstruction and are identified too if we consider a common 8-year length for the different periods (maximum length allowed for the 2016–2023 period) before and after the drops (Supplementary Table 5). The selected periods to define the drops could also be derived from a change point analysis (Supplementary Discussion).

The recent drop in Antarctic sea ice extent is well documented but the evaluation of our reconstructions is more difficult prior to 1979. Satellite observations from Electrically Scanning Microwave Radiometer (ESMR) instruments covering the period December 1972 to May 1977 have many gaps and a higher uncertainty than more recent satellite observations. Despite these limitations, data clearly indicate a sea ice extent decline over 1972–1977, and shows that the Antarctic sea ice extent during this period was considerably higher than in the 1980s[14,30,32]. A comparison performed for the years 1973 and 1974 (Fig. 2a), which have a sufficient data coverage, displays ESMR-based sea ice extents higher than in our reconstructions. However, from estimates with large uncertainties for only 2 years, we cannot reach more quantitative conclusions (see also Supplementary Fig. 4).

Our results can also be compared to other indirect reconstructions of the sea ice extent (i.e., not directly derived from sea ice observations). The

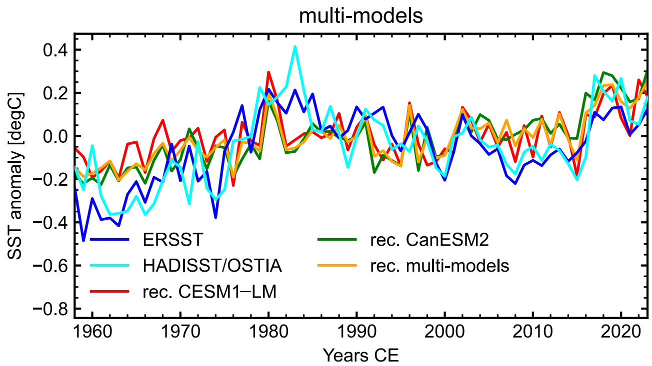

Fig. 3 | Sea surface temperature in the Southern Ocean. Reconstruction of the annual mean sea surface temperature averaged over the latitude band 50°-60°S in the multi-model reconstruction (in orange) and the reconstructions based on CESM1-LM (in red) and CanESM2 (in green) compared with estimates from direct observations derived from ERSST5[35] (in dark blue) and the SST dataset used in the ERA5 reanalysis (in cyan), which is based on HadISST2 until 2007 and OSTIA afterwards[26]. Anomalies are computed relative to the 1980–2015 period.

reconstruction of the sea ice extent of Fogt et al.[18] is based on long series of weather observations, mainly at mid-latitudes, using principal component regression techniques. Their reconstruction was calibrated using sea ice observations over the period 1979–2020 and adequately reproduces the impact of large-scale atmospheric circulation patterns on sea ice. The correlation over the period 1958–2020 with our multi-model reconstruction is higher than 0.59 for the Weddell and Amundsen/Bellingshausen Sea sectors but lower for the other sectors (Supplementary Fig. 3). For the total sea ice extent, the correlation with our reconstruction is still statistically significant but with a value of 0.35. Overall, the reconstruction of Fogt et al.[18] displays a weaker trend than our reconstruction. This difference is at least partially explained by our much larger network of high latitude data, in particular continental temperature records that strongly constrain the long-term trends[20] (Supplementary Fig. 5). Additionally, our reconstruction aligns with sea ice reconstructions obtained from paleoclimate records, which consistently show a sea ice extent decrease over the 20th century, except in the Ross Sea[17,19] (Supplementary Fig. 6).

The comparison with sea surface temperature (SST) data offers another way to determine if the drop in Antarctic Sea ice extent at the end of the 1970s is consistent with independent observations. The SST in the Southern Ocean exhibit a long-term trend (similar to, but opposite sign to the one of the Antarctic sea ice extent), characterized by warming between 1958 and 1980, followed by a slight cooling until around 2010 before the recent warming[33,34]. Our annual mean SST reconstructions are in good agreement with the observations (Fig. 3) although they tend to underestimate the warming trend between 1958 and 1980, in particular compared to ERSST5[35]. However, it is worth mentioning that this period has the fewest SST observations, and therefore large uncertainties exist.

Description of the changes associated with the drops in sea ice extent

The spatial distribution of the differences between the periods 1958–1979 and 1980–2015 and between the periods 1980–2015 and 2016–2023 (referred to hereafter as the first drop and the second drop) bears many similarities (Fig. 4). Although local changes in sea level pressure are not large compared to the interannual variability, both drops are characterized by a decrease in surface pressure over Antarctica and a strengthening of the Amundsen Sea Low (the ASL, a low-pressure system centered in the Amundsen Sea). This pattern is consistent with the observed trend in the SAM index and of the ASL since the mid-20 century[36,37].

The surface warming during the drops is more significant locally, with a pronounced temperature increase close to the Antarctic Peninsula. There is also a large warming off East Antarctica, specifically around 30°E, while the Ross Sea shows little or no warming. Consistently, sea ice decreases are larger in the regions displaying the largest temperature changes. Those patterns closely match those derived from NSIDC[29] and ERA5 reanalysis for the second drop (Supplementary Fig. 7).

Some differences also occur between the two drops. In particular, the low-pressure anomaly in the Amundsen Sea is located more eastward for the second drop. This low-pressure anomaly brings warm air from the north on its eastern side, amplifying the warming, and cold air from the south on its western side, partly offsetting the large-scale warming during the drops and leading to nearly no change there. The shift in the low-pressure anomaly between the two drops leads to an eastward displacement of the region with the largest warming and largest sea ice changes. Furthermore, the atmospheric circulation anomaly induces a large warming over the whole West Antarctic continent for the first drop but not for the more recent drop, in agreement with continental observations[38,39]. The pattern of the sea ice anomalies in the Pacific is thus consistent with the wind-driven changes associated with the ASL (Supplementary Fig. 8) that have been accredited extensively for interannual[40] and multidecadal variations[41]. The direct impact of the winds on sea ice extent changes is less clear off East Antarctica.

The comparison of oceanic temperatures in NEMO with observations[42,43] provides an additional independent validation of our results (Fig. 5). In the West Antarctic sector, NEMO overestimates the temperatures before 1980 (Fig. 5ac). There, the multidecadal variability is large, both in the top 100 m and in the 100–500 m depth range, with a long-term trend that is smaller than this multidecadal variability. The behavior is different in the East Antarctic sector where the top 100 m presents a time evolution that mimics the sea ice variability, as expected (Fig. 5b). However, the layer between 100 and 500 m (Fig. 5d) shows a nearly continuous warming over the whole period, both in NEMO and in observations.

Discussion

The reconstructed decline in sea ice extent since 1958 is consistent with the Southern Ocean warming[33,44] and the continental warming observed over most Antarctic stations during that period[38]. Our methodology establishes a physical link across those different changes in three different components of the climate system, i.e., the atmosphere, the sea ice and the ocean. Although such a reconstruction is not sufficient to quantitatively estimate the relative contribution of atmospheric and oceanic processes in the two drops, it suggests connections that can be compared to previous works and further tested in future studies. It also provides a useful test for the different datasets that we use as validation since these are themselves uncertain and the agreement with our independent estimates confirm the robustness of this general warming.

It can be tempting to attribute the warming in the atmosphere, in the ocean and the decrease in sea ice extent since 1958 to a long-term response to anthropogenic forcing, modulated by natural variability and regional processes. Furthermore, this reconstructed sea ice extent decrease since 1958 may appear more consistent with the climate model results (Supplementary Fig. 10) than when the model evaluation was made on shorter periods[1,13,45]. Nevertheless, the climate models have large biases in the Southern Ocean and they generally fail to reproduce adequately the observed sea ice variability, in particular the small increasing trend over 1979–2015[13,45]. Consequently, they cannot be used without additional validation for an attribution of the origin of the long-term sea ice decrease. Furthermore, the reconstructed period remains short considering the large natural variability prevailing in the Southern Ocean. Having estimates back to 1958 is an important step to characterize this variability but additional reconstructions of the sea ice extent before 1958 are needed before drawing conclusions on the magnitude of the natural and anthropogenic contributions in the trends since 1958. In this regard, combining paleo records with instrumental records is a promising way forward[19,20].

An influence of the Interdecadal Pacific Oscillation (IPO) over the Southern Ocean has been identified in several studies[10,25,44,46]. Specifically, the IPO has controlled the recent multidecadal variability of the sea surface temperature and oceanic heat content in the Pacific sector of the Southern

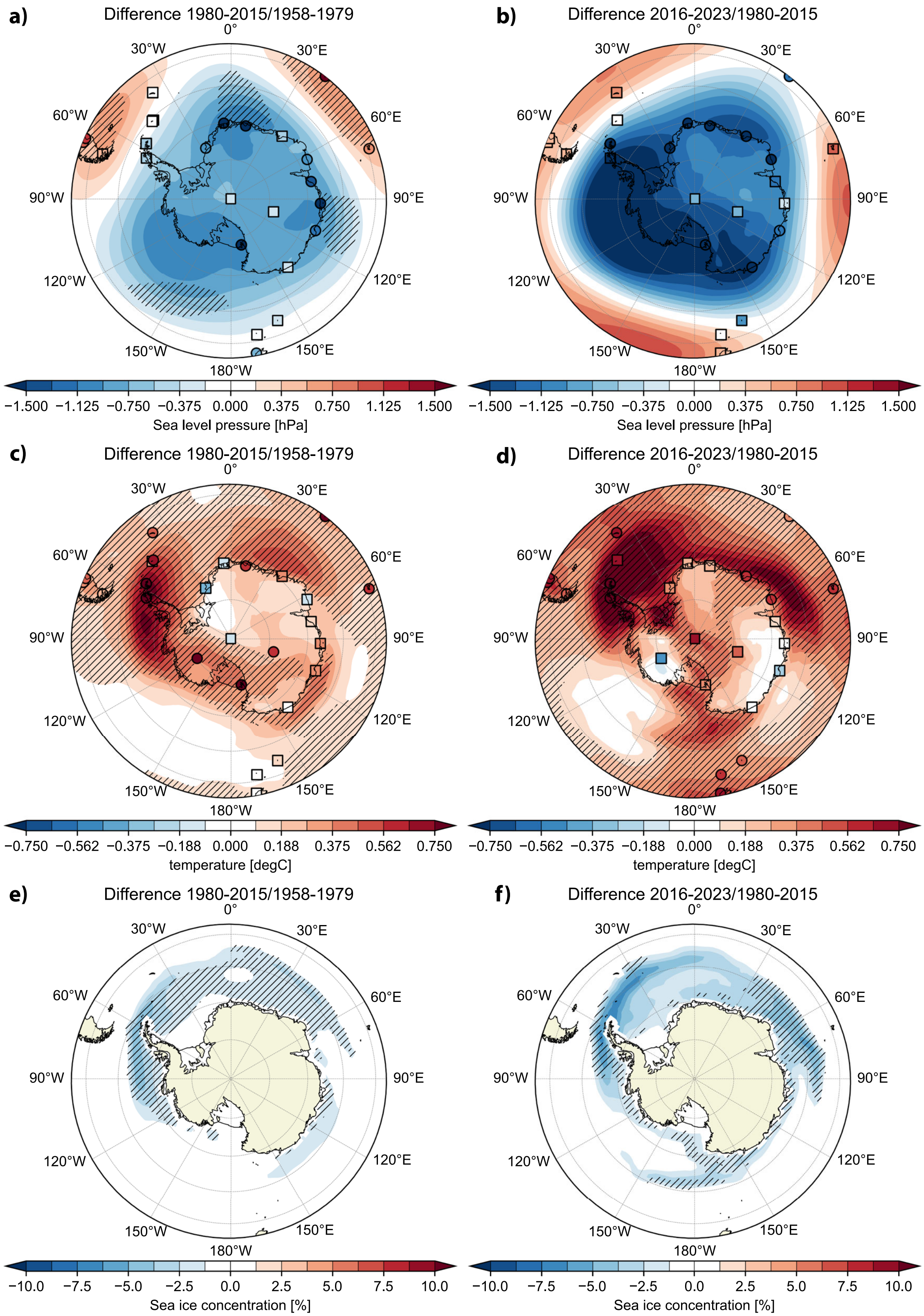

Fig. 4 | Shifts during the two drops. Difference in annual mean sea level pressure (**a**, **b**), near surface air temperature (**c**, **d**) and sea ice concentration (**e**, **f**) between the periods 1958–1979 and 1980–2015 (left column) and between the periods 1980–2015 and 2016–2023 (right column) in the multi-model reconstruction. Changes significant at the 90% level using a two-sided t-test accounting for the false discovery rate are hatched. Because of the large variability of the atmospheric circulation, only a few changes are statistically significant at the 90% level for sea level pressure, but many regions become significant if the confidence level is decreased to 80%. The anomalies from weather station data are indicated in colored circles if significant at the 90% confidence level and by a colored square if non-significant at the 90% confidence level.

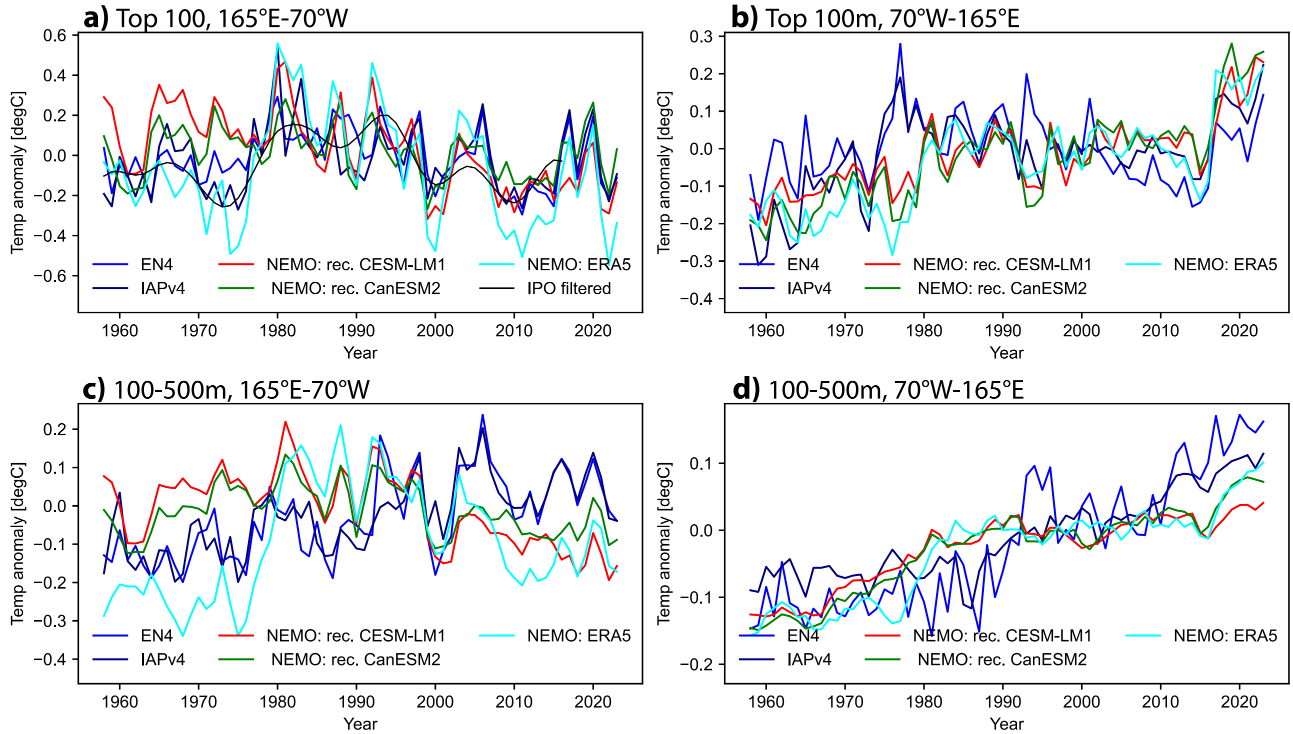

Fig. 5 | Evolution of the heat content of the Southern Ocean. Mean ocean temperature in the top 100 m (**a**, **b**) and in the layer from 100 m to 500 m (**c**, **d**) averaged over the latitude band 55–65°S for the West Antarctic sector of the Southern Ocean (165°E-70°W) and the East Antarctic sector of the Southern Ocean (70°W-165°E) in the NEMO simulations driven by the forcing derived from the CESM-LM1 reconstruction (in red), the CanESM2 reconstruction (in green) and ERA5 (in cyan) and in two datasets based on in situ observations (EN4[42] in light blue and IAPv4[43] in dark blue). The filtered IPO index (based on ERSSTv5 data[35]) has been added on panel a, scaled by a factor 2 to have an amplitude similar to other curves (in black).

Ocean[44,46]. It has also impacted the decadal variability of sea ice extent after 1979[25] and likely played a role in the drop in 2016[10]. Furthermore, tropical variability has a large impact on the ASL[24,40,46–48]. The IPO could thus influence the sea ice extent in the Pacific sector both through atmospheric and oceanic processes. In this framework, our results (Fig. 5a) suggest that the increase in the IPO index in the 1970s and the following decreasing trend could also partly explain the multidecadal variability in the sea ice extent in the West Antarctic sector before 1979 and the drop at the end of the 1970s.

It has been shown that the decrease in 2016 and subsequent minima were initiated by atmospheric circulation anomalies[1,3–8]. Wind changes could also be at the origin of the relatively stable conditions between 1979 and 2016[13,49–51]. Additionally, the ocean likely contributed to the recent decadal variability in Antarctic sea ice extent[3,10]: 1/ The ocean integrates the high frequency atmospheric forcing, sustaining the anomaly for a longer period and inducing lower frequency variations[52]. 2/ Oceanic feedbacks can be triggered by the atmospheric perturbations[1,53,54]. 3/ Specific oceanic processes such as changes in convection can be at the origin of decadal variability[55]. 4/ Meltwater input from the continent can modify the heat exchanges between the ocean and the sea ice and influence the multi-decadal variability of sea ice[51].

Our results also suggest a contribution of the winds in the drops, at least in their regional distribution and in particular in the Pacific sector (Supplementary Fig. 8). We have not addressed here the potential role of the meltwater input to the ocean. Our NEMO simulations show no evidence of change in oceanic convection but the multi-model reconstruction does not reproduce the opening of the large Weddell polynya between 1974 and 1976[56] so we may underestimate the role of this process. The better representation in the NEMO simulations than in the corresponding reconstructions of the magnitude of the second drop, of the 2023 minimum and of the autocorrelation of the sea ice extent series (see method section) strongly suggest a role of the integration of the atmospheric perturbations by the ice-ocean system and of the memory provided by the ocean. NEMO results are also consistent with a preconditioning by 2022 minimum of the 2023 minimum as suggested in previous studies[3,4]. This preconditioning led to the observed absolute minimum in the satellite area while our reconstructions based on the climate model ensembles indicate that the atmospheric conditions alone where not sufficient for such an absolute minimum. Finally, the thermal energy stored at depth between 1980 and 2015 in the East Antarctic sector (where the drop in sea ice extent is larger than in the West Antarctic sector, see Supplementary Table 4) has clearly the potential to induce a large sea ice melting if brought to the surface. The mixed layer depth in the model in the East Antarctic sector is larger after 2015 than before (Supplementary Fig. 9), inducing an entrainment in the top 100 m of warmer water from below. This may have contributed to maintain a warm condition in the top oceanic layer and could have initiated feedbacks with the sea ice and the atmosphere[53]. However, this cannot be to addressed here as our simulation with NEMO is not coupled with the atmosphere. Additional experiments and analyses are thus required to quantify precisely the contribution of the different processes and the various feedbacks in the multi-decadal variability of the Southern Ocean and to determine how the recent changes align with these multi-decadal variations. Our reconstruction, describing in a consistent way the changes in the atmosphere, ocean and sea ice, underlines that the coupling between the different components is a key element to this variability.

Methods

Method for reconstructing high latitude climate fields

The annual mean reconstruction is based on data assimilation using a particle filter, as applied in previous studies for reconstructions from paleoclimate records covering the past centuries[19,22,23]. An ensemble of simulations provides a distribution of the state of the system (the prior distribution). Each ensemble member (or particle) is compared to available observations for every year to estimate its likelihood. A weight is then given to each particle proportional to this likelihood for each year covered by the reconstruction. The weighted mean of all the particles provides the mean reconstruction while the range of the weighted ensemble (posterior distribution) gives an estimate of the uncertainty. This weighted mean can be applied to all the fields simulated by the model to obtain reconstructions for different variables, the covariance between locations and between variables in the reconstruction being based on model physics. Here, we use a prior fixed in time based on existing simulations, which is thus the same for each reconstructed year. This approach, which has been successful in many past applications[19,57], is often referred to as non-cycling or offline data assimilation. It has the advantage that it is cheap to obtain a large ensemble to characterize the prior distribution. The time evolution of the reconstruction is then provided by the data constraint only, the particle filter giving more weight to the particles in better agreement with the observations. Without this data constraint, the filter would give the same weight to all the particles and the reconstruction would provide a constant field equal to the ensemble mean of the simulations. This also means that the simulated trend in sea ice extent, which is biased in many models[45] does not have a direct impact on the reconstruction and that the reconstructed trend can thus be very different from the one in the prior (Supplementary Fig. 10).

Selected simulation results for the reconstruction

The model results used to build the prior consist in all the years of nine existing large ensembles of historical simulations performed with nine different climate models[21] (Supplementary Table 2). Particle filters have the risk of degeneracy when the number of particles is too low[22,23], justifying our choice here of large ensembles only. We have made tests with additional model ensembles but we did not obtain skillful reconstructions for the Antarctic sea ice extent, having either a non-significant correlation with satellite estimates of the sea ice extent or a negative coefficient of efficiency (CE[58]). This could be due either to a too small number of ensemble members or to an inadequate model covariance between the assimilated variables and sea ice concentration. Those large ensembles are thus not included here. For the simulations continuing after 2023, we limit the ensemble to the year 2023. The goal is to avoid to include states or covariance structures that may be too different from the ones observed over the past decades due to a larger response to anthropogenic forcings. A reconstruction is first obtained using each large ensemble separately, providing nine different reconstructions. The multi-model reconstruction corresponds to the mean of the nine reconstructions. Note that for our reconstructions, the sea ice extent is first calculated from monthly mean model results, before making the annual mean. For the other variables, the annual mean is simply the average of the monthly mean fields.

The nine ensembles display different simulated states in the Southern Ocean. In particular, their simulated sea ice extent ranges from a large underestimation to a large overestimation compared to observations (Supplementary Fig. 10). They provide thus a well-adapted sampling of the current climate model behavior[45]. Using all of them gives a strong test of the dependency of our conclusions to the selected model and thus of their robustness. However, because of these biases on the mean state, we use time anomalies in the assimilation (compared to the mean over the simulated period), and we cannot provide skillful reconstruction at the seasonal scale, in particular, in summer, when many models have nearly no sea ice left and thus could not provide information on the sea ice variability. Working with time anomalies is common practice for data assimilation-based reconstructions of climate variations beyond the satellite era[57]. No additional bias correction is applied to the model results.

Selected observations for the reconstruction

The data constraint is provided by weather station observations of near-surface air temperature and sea level (or station level) pressure, collected from the READER data set[59] and from the University Corporation for Atmospheric Research data archive dataset ds570.0 as in Fogt et al.[18]. Additionally, the temperature at Byrd station comes from Bromwich et al.[60]. As our goal is to reconstruct the climate of the high latitudes of the Southern Hemisphere, we have selected all the stations southward of 45°S for which data are available at least since 1961. We wanted to have a data set that is as homogenous in time as possible and having series starting later could introduce spurious biases in the reconstructed evolution. Actually, nearly all series goes back to 1958 except a few stations (Supplementary Table 1). This let us with data from 27 stations (Supplementary Fig. 11). In order to avoid regions with a dense station network having a too large influence on the final reconstruction, data within the same grid box of 500 × 500 km are averaged as in ref. 19. On a practical point of view, this only applies here to the stations Signy and Orcadas, McMurdo and Scott Base, Comodoro Rivadavia and Sarmiento, respectively. A special treatment is also performed for the Halley station where the different records from the slightly moving station location are merged to a single record. This may introduce a drift in the series[61] but the potential impact on our results is very small (Supplementary Fig. 12). The Neumayer and SANAE records are also merged. They are in the same 500 × 500 km box but cover different periods. However, the 10-year overlap is used to avoid any spurious shift between the two series. Data assimilation also requires to specify the data uncertainty of the records and the representativity of those records at the scale of the model grid. In the absence of specific information, we use an uncertainty of one standard deviation of the annual time series. Our results are not very sensitive to this choice (Supplementary Fig. 13).

Simulations with the model NEMO

A main limitation of the offline data assimilation method is that the reconstructions for different times are independent of each other: the reconstruction obtained at one time does not provide information for the reconstruction at the next time step and some inconsistencies between reconstructions for nearby periods can occur. Our reconstruction has an annual resolution. This means that this should not be a too large problem for air temperature or wind fields that have relatively low auto-correlation on annual time-scale but this is not valid for reconstructing ocean temperature at depths where the memory of the system is larger. To test the impact of this limitation for the sea ice variables and to provide estimates of the changes in oceanic variables, we have driven the sea-ice ocean model NEMO4.2 over the period 1958–2023 with a forcing derived from our reconstructions. The NEMO model[62] includes the OPA ocean model (Océan PArallélisé) coupled SI^3 sea ice model[63] and is run here at a global resolution 1°. To limit the number of simulations with NEMO, we only use the reconstructions based on CESM-LM and CanESM2 simulations that are among the most skillful ones (Supplementary Table 3) and that provide all the necessary fields to drive the model.

The data assimilation-based reconstructions deliver annual mean values for all the forcing fields but the standard NEMO forcing requires 6-hour values. Consequently, we first derived a mean climatological forcing based on the ERA5 forcing over the period 1981–2010 by subtracting to the original series the anomaly for each month compared to mean monthly value over the 30-year period. This provides a 30-year long series with the same seasonal cycle for each year but preserving the daily variations as in ref. 64. We then add the annual mean anomaly for each of the forcing field derived from our reconstruction for all the years of the period 1958–2023, distributing it over the different months proportionally to the mean amplitude of the anomalies for each month in the ERA5 reanalysis. The goal is to add larger anomalies to the months with the largest variance and to avoid unphysical values that would have appeared if we would have added the same value for each month, such as non-zero values for the solar radiation during the polar night for instance. We also discuss briefly a NEMO simulation driven by ERA5 forcing directly. To obtain initial states for the simulations over 1958–2023, we have first initialized the model from the Word Ocean Atlas[65] and performed three experiments driven by the ERA5 forcing over 1979–2023, the end of the simulation over 1979–2023 being the initial condition for the next one. From the state obtained in the third experiment in 2014, we have performed a simulation over 1958–1967 for each forcing, the state in 1968 being then the initial condition for the simulations analyzed here for each forcing.

Independent datasets for the validation of the reconstruction

To evaluate the skill of our reconstructions, they are compared to several datasets. The sea ice concentration is obtained from the National Snow and Ice Data Center (NSIDC) for the period 1979–2023[29]. Before 1979, other satellite observations are available but the temporal coverage can be insufficient to provide annual mean anomalies. Observations from the Electrically Scanning Microwave Radiometer (ESMR) instrument on board of the NIMBUS 5 satellite cover the period December 1972- May 1977 but have many gaps, in particular after June 1975. Consequently, we only show here the values for 1973 (8 monthly means available) and 1974 (12 monthly means available). We use a recent reevaluation of ESMR observations that provides extent on average 0.59 million km^2 larger than previous estimates based on the same data[32]. To estimate the annual mean, we compute the monthly mean anomaly relative to NSIDC data over 1979–2023 and then average the monthly anomalies.

HadISST2 sea ice concentration fields are based before 1979 on sea ice charts derived from ship observations and early satellite observations. Because of the data scarcity, the procedure to obtain continuous spatial maps implies gap filling, and time interpolations, with climatologies being applied for some decades when no information is available to determine interannual variations, leading to large uncertainties[16].

We also compare our reconstruction of sea ice extent for the five main sectors of the Southern Ocean to the ones of ref. 18 deduced from instrumental observations at weather stations and several climate indices, using a regression-based statistical method calibrated to satellite estimates of sea ice concentration. This reconstruction is seasonal as the teleconnections between mid and high latitudes are much larger at the seasonal scale than for annual means. We simply averaged the four seasons for the comparison with our reconstruction. Finally, we compare our sea ice extent reconstructions to the ones of ref. 19 based on paleoclimate records using the same data assimilation technique as in the present study.

The ERA5 atmospheric reanalysis provides estimates of atmospheric fields for the period 1940–2023. While ERA5 is generally considered as the best available reanalysis for Antarctica[66], its performance is lower before 1979 as many satellite observations begin only after this date. In particular, a cold bias before 1979 has been observed for several stations, likely because of a misrepresentation of the sea ice concentration in the surface boundary condition applied in the reanalysis[27,28] (Supplementary Fig. 4). Consequently, we only evaluate our reconstructions by comparing them to ERA5 data for the post-1979 period. Besides, as the same observation network is applied for the whole period covered by our reconstructions, they could potentially be used to detect spurious trends in ERA5 associated with the changes in the amount of observations used as constraint. Additionally, we compare our reconstruction of the SAM index to the one of ref. 36 derived from station observations of sea level pressure.

For the evaluation of sea surface temperature, we use ERSSTv5[35] and the dataset created to obtain the surface boundary conditions in ERA5, which is based on HADISST2 and OSTIA data[26]. A sea ice masking algorithm is applied in those SST data that requires estimates of the sea ice concentration, which are very uncertain before 1979 as discussed above[35]. Consequently, we have selected for our diagnostics the latitude band 50°S-60°S as it is well in our domain of interest while still keeping a data coverage that is good enough to estimate the general trend in zonal mean sea surface temperature over the period 1958–2023[35,67]. For the ocean temperature at depth, we have selected EN4[42] and IAPv4[43], which are long, objective analyses of oceanic data, including corrections to account for the biases introduced by the application of different sensors over time.

NSIDC, ESMR and oceanic data provide independent information to evaluate our reconstructions. The ERA5 reanalysis, Fogt et al.[18] sea ice reconstruction and the Marshall index share some data with us. Nevertheless, ERA5 includes much more data than the 27 stations selected here. Fogt et al.[18] only selected station data going back to the beginning of the 20th century meaning that the only Antarctic station in common with our reconstruction is Orcadas. The Marshall index uses some of the stations selected here but also additional ones at mid-latitudes.

The comparison with those additional data sets illustrates the general performance of our methodology as discussed in the main text and also some specific limitations that are mentioned here. First, as the reconstruction relies on model covariance, biases in this covariance reduces the performance of the reconstruction, in particular in regions where few data are available such as the Ross–Amundsen Seas sector (165°E–110°W). Consequently, for models that are able to reproduce well the links between changes there and in other regions where more data is available, reconstructions have a correlation with observed sea ice extent larger than 0.6 while some other reconstructions have correlations very close to zero (Supplementary Table 3). Second, the particle filter is not able to reconstruct states that are out of the range of the simulate ensemble (i.e., the prior). We try to mitigate the consequences of this limitation by selecting large ensembles and ensembles with different models. Nevertheless, this likely contribute to the underestimation of the largest anomalies in our sea ice extent reconstructions (Fig. 2). Third, offline data assimilation may underestimate the autocorrelation of the observed series as reconstructions of different years are independent. Analyses of observations[4] have shown that the autocorrelation of the time series of sea ice extent was low until 2008 and increases strongly after that. Our reconstructions reproduce qualitatively well this behavior, with autocorrelation at lag 1 year of the Antarctic sea ice extent close to zero for the period 1979–2008, as in the observations, and a value for the multi-model reconstruction of 0.27 for the period 1979–2023. However, this is much less than the observations that show an autocorrelation at lag 1 year of 0.61 over the same period. Thanks to the contribution of the ocean, the autocorrelation of the sea ice extent over 1979–2023 in two NEMO simulations rises to 0.32 and 0.42 but this is still a large underestimation.

Reporting summary

Further information on research design is available in the Nature Portfolio Reporting Summary linked to this article.

Data availability

All the data used were obtained from public repositories. The weather station observations were obtained from the READER data set (https://legacy.bas.ac.uk/met/READER/) and from the University Corporation for Atmospheric Research data archive dataset ds570.0 (https://rda.ucar.edu/datasets/ds570.0/#!description). The temperature at Byrd station is available at https://polarmet.osu.edu/datasets/Byrd_recon/. The ERA5 reanalysis, including its surface boundary conditions, has been downloaded from the Copernicus Climate Change Service (C3S) Climate Data Store[68]. ERSSTv5[69] is available at https://downloads.psl.noaa.gov/Datasets/noaa.ersst.v5/. EN.4.2.2 data was obtained from https://www.metoffice.gov.uk/hadobs/en4/ and are © British Crown Copyright, Met Office, 2024, provided under a Non-Commercial Government Licence http://www.nationalarchives.gov.uk/doc/non-commercial-government-licence/version/2/. IAP data were obtained from the IAP/CAS website http://www.ocean.iap.ac.cn/pages/dataService/dataService.html?navAnchor=dataService). Sea-ice concentration data set from the NSIDC[29], ESMR[70], the sea-ice extent reconstruction of Fogt et al.[71]. and Dalaiden et al.[72]. the Marshall index[73] are available in dedicated repositories (see the refences). Our reconstructions are available on Zenodo https://zenodo.org/records/13861997.

Code availability

NEMO and XIOS (a NEMO-compatible I/O library) are developed by the NEMO consortium (https://www.nemo-ocean.eu/) and distributed under the CeCILL license (http://cecill.info/licences/Licence_CeCILL_V2-en.txt). The code for the particle filter assimilation system is available here https://github.com/dalaiden/DA_offline_PF.

Received: 18 June 2024; Accepted: 15 October 2024;
Published online: 25 October 2024

References

1. Hobbs, W. R. et al. A review of recent changes in Southern Ocean sea ice, their drivers and forcings. *Glob. Planet. Change* **143**, 228–250 (2016).
2. Parkinson, C. L. & DiGirolamo, N. E. Sea ice extents continue to set new records: Arctic, Antarctic, and global results. *Remote Sens. Environ.* **267**, 112753 (2021).
3. Purich, A. & Doddridge, E. W. Record low Antarctic sea ice coverage indicates a new sea ice state. *Commun. Earth Environ.* **4**, 314 (2023).
4. Hobbs, W. et al. Observational evidence for a regime shift in summer Antarctic sea ice. *J. Clim.* https://doi.org/10.1175/JCLI-D-23-0479.1 (2024).
5. Stuecker, M. F., Bitz, C. M. & Armour, K. C. Conditions leading to the unprecedented low Antarctic sea ice extent during the 2016 austral spring season. *Geophys. Res. Lett.* **44**, 9008–9019 (2017).
6. Schlosser, E., Haumann, F. A. & Raphael, M. N. Atmospheric influences on the anomalous 2016 Antarctic sea ice decay. *Cryosphere* **12**, 1103–1119 (2018).
7. Wang, Z., Turner, J., Wu, Y. & Liu, C. Rapid decline of total Antarctic sea ice extent during 2014-16 controlled by wind-driven sea ice drift. *J. Clim.* **32**, 5381–5395 (2019).
8. Turner, J. et al. Record low Antarctic sea ice cover in February 2022. *Geophys. Res. Lett.* **49**, e2022GL098904 (2022).
9. Polvani, L. M. et al. Interannual SAM modulation of Antarctic sea ice extent does not account for its long-term trends, pointing to a limited role for ozone depletion. *Geophys. Res. Lett.* **48**, e2021GL094871 (2021).
10. Meehl, G. A. et al. Sustained ocean changes contributed to sudden Antarctic sea ice retreat in late 2016. *Nat. Commun.* **10**, 14 (2019).
11. Zhang, L. et al. The relative role of the subsurface Southern Ocean in driving negative Antarctic Sea ice extent anomalies in 2016–2021. *Commun. Earth Environ.* **3**, 302 (2022).
12. Suryawanshi, K., Jena, B., Bajish, C. C. & Anilkumar, N. Recent decline in Antarctic sea ice cover from 2016 to 2022: insights from satellite observations, argo floats, and model reanalysis. *Tellus A: Dyn. Meteorol. Oceanogr.* **75**, 193–212 (2023).
13. Jones, J. M. et al. Assessing recent trends in high-latitude Southern Hemisphere surface climate. *Nat. Clim. Change* **6**, 917–926 (2016).
14. Kukla, G. & Gavin, J. Summer ice and carbon dioxide. *Science* **214**, 497–503 (1981).
15. de la Mare, W. K. Changes in Antarctic sea-ice extent from direct historical observations and whaling records. *Clim. Chang.* **92**, 461–493 (2009).
16. Titchner, H. A. & Rayner, N. A. The Met Office Hadley Centre sea ice and sea surface temperature data set, version 2: 1. Sea ice concentrations. *J. Geophys. Res. Atmos.* **119**, 2864–2889 (2014).
17. Thomas, E. R. et al. Antarctic Sea Ice Proxies from marine and ice core archives suitable for reconstructing sea ice over the past 2000 years. *Geosciences*. https://doi.org/10.3390/geosciences9120506 (2019).
18. Fogt, R. L., Sleinkofer, A. M., Raphael, M. N. & Handcock, M. S. A regime shift in seasonal total Antarctic sea ice extent in the twentieth century. *Nat. Clim. Change* **12**, 54–62 (2022).
19. Dalaiden, Q. et al. An unprecedented sea ice retreat in the Weddell Sea driving an overall decrease of the Antarctic sea-ice extent over the 20th century. *Geophys. Res. Lett.* **50**, e2023GL104666 (2023).
20. Fogt, R. L., Dalaiden, Q. & O'Connor, G.K. A comparison of South Pacific Antarctic sea ice and atmospheric circulation reconstructions since 1900. *Clim. Past* **20**, 53–76 (2024).
21. Deser, C. et al. Insights from Earth system model initial-condition large ensembles and future prospects. *Nat. Clim. Change* **10**, 277–286 (2020).
22. van Leeuwen, P. J. Particle filtering in geophysical systems. *Monthly Weather Rev.* **137**, 4089–4114 (2009).
23. Dubinkina, S., Goosse, H., Sallaz-Damaz, Y., Crespin, E. & Crucifix, M. Testing a particle filter to reconstruct climate changes over the past centuries. *Int. J. Bifurc. Chaos* **21**, 3611–3618 (2011).
24. Stammerjohn, S. E., Martinson, D. G., Smith, R. C., Yuan, X. & Rind, D. Trends in Antarctic annual sea ice retreat and advance and their relation to El Niño–Southern Oscillation and Southern Annular Mode variability. *J. Geophys. Res.* https://doi.org/10.1029/2007JC004269 (2008).
25. Bonan, D. B., Dörr, J., Wills, R. C. J., Thompson, A. F. & Årthun, M. Sources of low-frequency variability in observed Antarctic sea ice. *Cryosphere* **18**, 2141–2159 (2024).
26. Hersbach, H. et al. The ERA5 global reanalysis. *Q. J. R. Meteorol. Soc.* **146**, 1999–2049 (2020).
27. Bell, B. et al. The ERA5 global reanalysis: preliminary extension to 1950. *Q. J. R. Meteorol. Soc.* **147**, 4186–4227 (2021).
28. Lu, H. et al. Temperature variation in the South Orkney Islands, maritime Antarctic. 10.1002/joc.8302 (2023).
29. NSIDC. Satelitte sea-ice concentration product [Dataset]. NSIDC. Retrieved from https://nsidc.org/data/NSIDC-0051/versions/1 (2023).
30. Cavalieri, D. J., Parkinson, C. L. & Vinnikov, K. Y. 30-Year satellite record reveals contrasting Arctic and Antarctic decadal sea ice variability. *Geophys. Res. Lett.* **30**, 1970 (2003).
31. Comiso, J. C. & Nishio, F. Trends in the sea ice cover using enhanced and compatible AMSR-E, SSM/I, and SMMR data. *J. Geophys. Res.* **113**, C02S07 (2008).
32. Kolbe, W. M., Tonboe, R. T. & Stroeve, J. Mapping of sea ice concentration using the NASA NIMBUS 5 Electrically Scanning Microwave Radiometer data from 1972–1977. *Earth Syst. Sci. Data* **16**, 1247–1264 (2024).
33. Fan, T., Deser, C. & Schneider, D. P. Recent Antarctic sea ice trends in the context of Southern Ocean surface climate variations since 1950. *Geophys. Res. Lett.* **41**, 2419–2426 (2014).
34. Dong, Y., Polvani, L. M. & Bonan, D. B. Recent multi-decadal Southern Ocean surface cooling unlikely caused by Southern Annular Mode trends. *Geophys. Res. Lett.* **50**, e2023GL106142 (2023).
35. Huang, B. et al. Extended reconstructed sea surface temperature version 5 (ERSSTv5), upgrades, validations, and intercomparisons. *J. Clim.* **30**, 8179–8205 (2017).
36. Marshall, G. J. Trends in the southern annular mode from observations and reanalyses. *J. Clim.* **16**, 4134–4143 (2003).
37. Dalaiden, Q., Schurer, A. P., Kirchmeier-Young, M. C., Goosse, H. & Hegerl, G. C. West Antarctic surface climate changes since the mid-20th century driven by anthropogenic forcing. *Geophys. Res. Lett.* **49**, e2022GL099543 (2022).
38. Jones, M. E. et al. Sixty years of widespread warming in the Southern Middle and High Latitudes (1957–2016). *J. Clim.* **32**, 6875–6898 (2019).
39. Xin, M. et al. West-warming East-cooling trend over Antarctica reversed since early 21st century driven by large-scale circulation variation. *Environ. Res. Lett.* **18**, 064034 (2023).
40. Raphael, M. N. et al. The Amundsen Sea Low: variability, change and impact on Antarctic climate. *Bull. Am. Met Soc.* **97**, 111–121 (2016).
41. Dalaiden, Q., Goosse, H., Rezsohazy, J. & Thomas, E. R. Reconstructing atmospheric circulation and sea-ice extent in the West Antarctic over the past 200 years using data assimilation. *Clim. Dyn.* **57**, 3479–3503 (2021).
42. Good, S. A., Martin, M. J. & Rayner, N. A. EN4: quality controlled ocean temperature and salinity profiles and monthly objective analyses with uncertainty estimates. *J. Geophys. Res. Oceans* **118**, 6704–6716 (2013).
43. Cheng, L. et al. Improved estimates of ocean heat content from 1960 to 2015. *Sci. Adv.* **3**, e1601545 (2017).
44. Song, Y. et al. Decadal thermal variability of the upper Southern Ocean: zonal asymmetry. *J. Clim.* **37**, 3117–3132 (2024).
45. Roach, L. A. et al. Antarctic sea ice area in CMIP6. *Geophys. Res. Lett.* **47**, 1–24 (2020).
46. Yao, S. L. et al. Competing impacts of tropical Pacific and Atlantic on Southern Ocean inter-decadal variability. *npj Clim. Atmos. Sci.* **7**, 104 (2024).

47. Fogt, R. L. et al. A twentieth century perspective on summer Antarctic pressure change and variability and contributions from tropical SSTs and ozone depletion. *Geophys. Res. Lett.* **44**, 9918–9927 (2017).
48. Purich, A. & England, M. H. Tropical teleconnections to Antarctic sea ice during austral spring 2016 in coupled pacemaker experiments. *Geophys. Res. Lett.* https://doi.org/10.1029/2019GL082671 (2019).
49. Ferreira, D., Marshall, J., Bitz, C. M., Solomon, S. & Plumb, A. Antarctic Ocean and sea ice response to ozone depletion: a two-time-scale problem. *J. Clim.* **28**, 1206–1226 (2015).
50. Blanchard-Wrigglesworth, E., Roach, L. A., Donohoe, A. & Ding, Q. Impact of winds and Southern Ocean SSTs on Antarctic sea ice trends and variability. *J. Clim.* **34**, 1–47 (2021).
51. Roach, L. A. et al. Winds and meltwater together lead to Southern Ocean surface cooling and sea ice expansion. *Geophys. Res. Lett.* **50**, e2023GL105948 (2023).
52. Bitz, C., Battisti, D., Moritz, R. & Beesley, J. Low-frequency variability in the Arctic atmosphere, sea ice, and upper-ocean climate system. *J. Clim.* **9**, 394–408 (1996).
53. Goosse, H. et al. Quantifying climate feedbacks in polar regions. *Nat. Commun.* **9**, 1919 (2018).
54. Lecomte, O. et al. Vertical ocean heat redistribution sustaining sea-ice concentration trends in the Ross Sea. *Nat. Commun.* **8**, 258 (2017).
55. Zhang, L., Delworth, T. L., Cooke, W. & Yang, X. Natural variability of Southern Ocean convection as a driver of observed climate trends. *Nat. Clim. Change* **9**, 59–65 (2019).
56. Carsey, F. D. Microwave observation of theWeddell Polynya. *Mon. Weather Rev.* **108**, 2032–2044 (1980).
57. Hakim, G. J. et al. The last millennium climate reanalysis project: framework and first results. *J. Geophys. Res.* **121**, 6745–6764 (2016).
58. Nash, J. & Sutcliffe, J. River flow forecasting through conceptual models part I—a discussion of principles. *J. Hydrol.* **10**, 282–290 (1970).
59. Turner, J. et al. The SCAR READER project: toward a high-quality database of mean Antarctic meteorological observations. *J. Clim.* **17**, 2890–2898 (2004).
60. Bromwich, D. et al. Central West Antarctica among the most rapidly warming regions on Earth. *Nat. Geosci.* **6**, 139–145 (2013).
61. King, J. C. et al. Inhomogeneity of the surface air temperature record from Halley, Antarctica. *J. Clim.* **34**, 4771–4783 (2021).
62. Madec, G. and the NEMO System Team. NEMO Ocean Engine Reference Manual, Zenodo, https://doi.org/10.5281/zenodo.8167700 (2023).
63. Vancoppenolle, M., Rousset, C., Blockley, E., and the NEMO Sea Ice Working Group, 2023. SI3 – Sea Ice modelling Integrated Initiative – The NEMO Sea Ice Engine, Zenodo, https://doi.org/10.5281/zenodo.7534900 (2023).
64. Naughten, K. A. et al. Intercomparison of Antarctic ice-shelf, ocean, and sea-ice interactions simulated by MetROMS-iceshelf and FESOM 1.4. *Geosci. Model Dev.* **11**, 1257–1292 (2018).
65. Locarnini, R. A. et al. World Ocean Atlas 2013, Volume 1: Temperature. S. L., Ed.; A. Mishonov, Technical Ed.; NOAA Atlas NESDIS 73, 40 pp. publication 10.7289/V55X26VD, dataset (2013).
66. Gossart, A. et al. An evaluation of surface climatology in state-of-the-art reanalyses over the Antarctic Ice Sheet. *J. Clim.* **32**, 6899–6915 (2019). 2019pp.
67. Favier, V. et al. Atmospheric drying as the main driver of dramatic glacier wastage in the southern Indian Ocean. *Sci. Rep.* **6**, 32396 (2016).
68. Hersbach, H. et al. ERA5 hourly data on pressure levels from 1940 to present [Dataset]. Copernicus Climate Change Service (C3S) Climate Data Store (CDS). Retrieved from https://cds.climate.copernicus.eu/cdsapp#!/dataset/reanalysis-era5-single-levels?tab=overview (2020).
69. Huang, B. et al. NOAA Extended Reconstructed Sea Surface Temperature (ERSST), Version 5. NOAA National Centers for Environmental Information. https://doi.org/10.7289/V5T72FNM. Obtain at NOAA/ESRL/PSD at their website https://www.esrl.noaa.gov/psd/ 2024 (2017b).
70. Tonboe, R. T. et al. ESA Sea Ice Climate Change Initiative (Sea_Ice_cci): Nimbus- 5 ESMR Sea Ice Concentration, version 1.0., NERC EDS Centre for Environmental Data Analysis [data set], https://doi.org/10.5285/34a15b96f1134d9e95b9e486d74e49cf (2023).
71. Fogt, R. L., Sleinkofer, A. M., Raphael, M. N. & Handcock, M. S. Instrumental-based sea-ice extent reconstruction over the 20th century [Dataset]. figshare. Retrieved from https://figshare.com/collections/Antarctic_Sea_Ice_Reconstructions/5709767/1 (2023).
72. Dalaiden, Q. et al. Reconstructed sea ice and winds [Dataset]. Zenodo. (2023).
73. Marshall, G. Southern annular mode index from Gareth Marshall [Dataset]. Legacy. Retrieved from https://legacy.bas.ac.uk/met/gjma/sam.html (2003).

Acknowledgements

We acknowledge the World Climate Research Program's Working Group on Coupled Modeling, which is responsible for CMIP. For CMIP the US Department of Energy's Program for Climate Model Diagnosis and Intercomparison provides coordinating support and led development of software infrastructure in partnership with the Global Organization for Earth System Science Portals. H.G. is a Research Director and QD and BM are Research Fellows within the F.R.S.-FNRS (Belgium). This work was performed in the framework of the PDR project T.0101.22 "Role of WINDS and oceanic interactions on Sea ice Changes in the SOuthern Ocean over the Past millennium (WindSCOOP)" of the FRS-FNRS.

Author contributions

H.G. and Q.D. initiated the study and designed the experiments after discussions with all the co-authors. H.G., Q.D. and R.F. discussed the selection of the data. H.G. performed the reconstructions and Q.D. the simulations with NEMO. H.G., Q.D., F.F. and B.M. made the analyses and the figures, and all the co-authors contributed in the interpretation of the results. H.G. wrote the initial version of the manuscript, with inputs from all co-authors for the subsequent versions.

Competing interests

The authors declare no competing interests.

Additional information

Supplementary information The online version contains supplementary material available at https://doi.org/10.1038/s43247-024-01793-x.

Correspondence and requests for materials should be addressed to Hugues Goosse.

Peer review information *Communications Earth & Environment* thanks Ariaan Purich, Edward Doddridge and the other, anonymous, reviewer(s) for their contribution to the peer review of this work. Primary Handling Editor: Alireza Bahadori. A peer review file is available.